

**Impaired Resection of Meiotic
Double-Strand Breaks Channels Repair to
Nonhomologous End Joining in
*Caenorhabditis elegans***

Yizhi Yin and Sarit Smolikove
Mol. Cell. Biol. 2013, 33(14):2732. DOI:
10.1128/MCB.00055-13.
Published Ahead of Print 13 May 2013.

Updated information and services can be found at:
<http://mcb.asm.org/content/33/14/2732>

SUPPLEMENTAL MATERIAL

These include:

[Supplemental material](#)

REFERENCES

This article cites 62 articles, 31 of which can be accessed free
at: <http://mcb.asm.org/content/33/14/2732#ref-list-1>

CONTENT ALERTS

Receive: RSS Feeds, eTOCs, free email alerts (when new
articles cite this article), [more»](#)

Information about commercial reprint orders: <http://journals.asm.org/site/misc/reprints.xhtml>
To subscribe to to another ASM Journal go to: <http://journals.asm.org/site/subscriptions/>

Impaired Resection of Meiotic Double-Strand Breaks Channels Repair to Nonhomologous End Joining in *Caenorhabditis elegans*

Yizhi Yin, Sarit Smolikove

Department of Biology, University of Iowa, Iowa City, Iowa, USA

Repair of double-strand DNA breaks (DSBs) by the homologous recombination (HR) pathway results in crossovers (COs) required for a successful first meiotic division. Mre11 is one member of the MRX/N (Mre11, Rad50, and Xrs2/Nbs1) complex required for meiotic DSB formation and for resection in *Saccharomyces cerevisiae*. In *Caenorhabditis elegans*, evidence for the MRX/N role in DSB resection is limited. We report the first separation-of-function allele, *mre-11(iow1)* in *C. elegans*, which is specifically defective in meiotic DSB resection but not in formation. The *mre-11(iow1)* mutants displayed chromosomal fragmentation and aggregation in late prophase I. Recombination intermediates and crossover formation was greatly reduced in *mre-11(iow1)* mutants. Irradiation-induced DSBs during meiosis failed to be repaired from early to middle prophase I in *mre-11(iow1)* mutants. In the absence of a functional HR, our data suggest that some DSBs in *mre-11(iow1)* mutants are repaired by the nonhomologous end joining (NHEJ) pathway, as removing NHEJ partially suppressed the meiotic defects shown by *mre-11(iow1)*. In the absence of NHEJ and a functional MRX/N, meiotic DSBs are channeled to EXO-1-dependent HR repair. Overall, our analysis supports a role for MRE-11 in the resection of DSBs in middle meiotic prophase I and in blocking NHEJ.

Meiotic recombination is initiated by the formation of meiotic double-strand breaks (DSBs), which are then repaired by the meiotic homologous recombination (HR) pathway. A meiosis protein, SPO-11, along with other auxiliary proteins catalyzes the formation of meiotic DSBs and remains covalently bound to the 5' ends of the DSBs (1). These DSBs are converted to long 3' single-stranded DNA (ssDNA) by a process called resection. Meiotic DSB resection is initiated by endonuclease activity to release oligonucleotide-bound SPO-11 and generate a short 3' overhang (2). The short 3' overhang is further processed by a 5'-3' exonuclease activity to generate long 3' ssDNA (3, 4). The ssDNA is rapidly bound by the ssDNA binding protein RPA, which is then displaced by RAD-51, forming a filament that coats the ssDNA (5). RAD-51 then mediates the invasion of the ssDNA into the homologous double-strand DNA (dsDNA) (6, 7). Using the homologous sequence as the template, new DNA is synthesized from the invading 3' ends to fill in the region lost by end resection. Ligation of the invading strands forms a double Holliday junction (dHJ), which can be resolved to form crossovers (COs) (8). COs connect the homologous pairs of chromosomes, enabling their biorientation toward opposite spindle poles in metaphase I.

Mre11 acts in the context of the MRX/N complex, which is composed of Mre11, Rad50, and Nbs1/Xrs2. The MRX/N complex has dual roles in the early steps of the HR pathway in some organisms. First, MRX/N acts as a cofactor for Spo11 and is required for meiotic DSB formation in *Saccharomyces cerevisiae* (9). Second, MRX/N is required for the resection of meiotic DSBs in *S. cerevisiae*, *Schizosaccharomyces pombe*, and *Arabidopsis* sp. (10–13). The N terminus of the Mre11 protein contains five evolutionarily conserved phosphoesterase motifs responsible for the endonuclease and 3'-5' exonuclease activity of the Mre11 protein (10, 14–16). Point mutations in those motifs disrupt the MRX/N complex function in DSB resection but not in DSB formation (10, 14–16). The endonuclease activity of Mre11 is critical for the initiation of DSB resection and the removal of SPO-11 in meiosis (2, 10, 15–18). The 3'-5' exonuclease activity of Mre11 is implicated

in further resection of DSB ends in addition to other 5'-3' exonucleases, such as Exo1 and Dna2 (3, 4, 19). In contrast to evidence from yeast, the meiotic function of MRX/N in metazoan systems is poorly understood, due to the lethality caused by the disruption of these genes (20–23). The study of a nuclease-deficient allele of Mre11 in mice suggests a role for MRX/N in DSB resection in mitosis (24). However, little is known about MRX/N complex function in meiosis in these organisms.

An alternative mechanism for repair of DSBs is the nonhomologous end joining (NHEJ) pathway, which results in random joining of two dsDNA ends. This pathway is initiated by the binding of the Ku70/Ku80 heterodimer to dsDNA ends. Ku70/80 binding serves to protect the dsDNA ends from degradation as well as recruit DNA ligase IV and its accessory proteins. Ligase IV can then join DNA ends regardless of their homology (25). NHEJ is an error-prone pathway that frequently results in addition or removal of base pairs and/or chromosomal rearrangement (26–28). The NHEJ pathway is used primarily in the G₁ phase of the cell cycle, when a homolog or sister chromatid is not nearby (29). The role of the MRX/N complex in NHEJ is controversial. The MRX/N complex, but not its nuclease activity, has been implicated in the NHEJ pathway for repair of mitotic DSBs in *S. cerevisiae* (16, 28, 30). However, evidence suggests that the MRX/N complex is not required for NHEJ in *S. pombe* and vertebrates (31, 32). In *Caenorhabditis elegans*, NHEJ is exclusively used in nondividing somatic

Received 12 January 2013 Returned for modification 7 February 2013

Accepted 9 May 2013

Published ahead of print 13 May 2013

Address correspondence to Sarit Smolikove, sarit-smolikove@uiowa.edu.

Supplemental material for this article may be found at <http://dx.doi.org/10.1128/MCB.00055-13>.

Copyright © 2013, American Society for Microbiology. All Rights Reserved.

doi:10.1128/MCB.00055-13

cells for DNA repair, but normally it is not active in germ line cells (33). Nevertheless, NHEJ has been shown in *C. elegans* to repair meiotic DSBs in the germ line when HR is not available (34, 35).

In *C. elegans*, MRX/N is required to form meiotic DSBs, since mutants defective for Mre11 or Rad50 show no recombination intermediates as defined by the presence of RAD-51 or crossover formation and the finding that chromosomes remain intact (36, 37). These phenotypes are indistinguishable from those of *spo-11* null mutants, indicating a great reduction in meiotic DSB formation (37, 38). However, unlike *spo-11* mutants, the introduction of exogenous DSBs into *mre-11* or *rad-50* null mutants fails to restore crossovers and results in chromosomal fragmentation and aggregation at diakinesis, similar to mutants that are perturbed in later stages of meiotic DSB repair (e.g., *rad-51*, *com-1*, or *Cebrc-2* [34, 39, 40]). These studies suggest a role for MRX/N downstream of DSB formation in the repair of exogenous DSBs (36, 37). This downstream role may be specific to irradiation-induced DSBs, since meiotic DSBs have a distinct structure (i.e., SPO-11 is covalently bound to the 5' end of the DSBs).

Here we report the analysis of meiotic recombination in *mre-11(iow1)*, the first separation-of-function allele of *mre-11* in *C. elegans*, which is competent to form meiotic DSBs but not process them. Our analysis indicated that in the presence of a defective MRX/N, some meiotic DSBs are repaired via NHEJ. In the absence of a functional MRX/N and NHEJ, an EXO-1-dependent resection becomes active in middle to late prophase I. This EXO-1-mediated resection can partially bypass the requirement of MRX/N.

MATERIALS AND METHODS

Strains. All *C. elegans* strains were cultured under standard conditions at 20°C (60). Strain N2 worms were utilized as the wild-type background, while Hawaiian CB4856 wild-type worms were used for single-nucleotide polymorphism (SNP) mapping in the process of mapping *mre-11(iow1)*. The following mutations and chromosome rearrangements were used (33, 38, 46, 51): LGIII, *cKu-80(ok861)*, *exo-1(tm1842)*; LGIV, *spo-11(ok79)*, *msh-5(me23)*, *him-6(ok4128)*, *rad-51(lg8701)*, *nT1[qIs50]* (IV, V); and LGV, *mre-11(ok179)*, *mre-11(iow1)*. The following transgenic line was used (49, 61): *opIs263(RPA-1::YFP)*, *meIs8(GFP::COSA-1)*.

Isolation of *mre-11(iow1)*. We isolated the *iow1* allele in a forward genetic screen by using ethyl methanesulfonate as the mutagen. We screened for worms that showed a maternally rescued embryonic lethality, since worms with meiotic defects can survive to adulthood but fail to produce viable progeny. Then we performed a cytology-based secondary screen to identify worms with aberrant chromosome morphology at diakinesis. Allele *iow1* was linked to SNPs located in a region of chromosome V. In addition, *iow1* failed to complement *mre-11(ok179)*. The point mutation was identified by Sanger sequencing of the *mre-11* gene (including 5' and 3' untranslated regions [UTRs]), by using the following primers: forward primers GGATTCCAACATGCG AGATTGTAG, CAGTCTCGACGAGGAGACGAG, GCTACTTCGCTC ACTCCGGAAG, and GATAGGAATTGGAAGAGCTTTAGAGC and reverse primers CGCGATTGGATTCCCATCAAGC, CATCTATGTATC GGCCATCCGTGTG, GATCGTTAATCGGAGGCAGAGGC, and CACT CCCTAATAGTCTTGCACTCCC.

Western blotting. Rabbit anti-MRE-11 antibody was a generous gift from Simon Boulton. Adult homozygote worms were picked or selected via fluorescence-activated cell sorting (62). The rabbit anti-MRE-11 antibody was used as primary antibody (1:1,000). Mouse antitubulin (1:1,000; DSHB) was used as the loading control. Secondary antibodies used were anti-rabbit antibody conjugated to horseradish peroxidase (HRP; 1:10,000) and anti-mouse antibody-HRP. Tween-Tris-buffered saline (1×)-5% milk was used for incubation and blocking.

Apoptosis analysis. Germ cell corpses were scored in adult hermaphrodites 20 h post-L4 stage, as described in reference 46. Statistical comparisons between genotypes were performed using the two-tailed Mann-Whitney test, with 95% confidence intervals (CI).

Immunostaining and microscopy. Whole-worm preparation was performed as described in reference 42. Oocytes in whole-worm preparations were scored in adult hermaphrodites 20 h post-L4 stage. Immunostaining for RAD-51 and MRE-11 was performed as described in reference 42. Primary antibodies were rabbit anti-RAD-51 (1:10,000; ModEncode) and rabbit anti-MRE-11 (1:100; Simon Boulton). The secondary antibodies used were Alexa Fluor 488-anti-rabbit antibody (1:500) and Alexa Fluor 555-anti-rabbit antibody. YFP::RPA-1 and GFP::COSA-1 focus microscopy was performed as follows. Adult hermaphrodites 20 h post-L4 were dissected to release gonads on slides. Slides were frozen on dry ice and dipped into methanol for 1 min, followed by 15 min of fixation in 4% formaldehyde in the dark. Then, slides were washed in phosphate-buffered saline-Tween (PBST) for 5 min, stained with 4',6-diamidino-2-phenylindole (DAPI; 1:2,000 dilution of a 5-mg/ml DAPI stock in PBST) for 5 min, and washed in PBST for 5 min. Vectashield was added to slides.

The images were acquired using the DeltaVision wide-field fluorescence microscope system (Applied Precision) with Olympus 100×/1.40-numerical aperture lenses. Optical sections were collected at 0.20- μ m increments with a coolSNAP_{HQ} camera (Photometrics) and softWoRx software (Applied Precision) and deconvolved using softWoRx 5.0.0 software, except for Fig. S1 in the supplemental material, which is not deconvolved and is a single optical section. Images are projections through three-dimensional data stacks of whole nuclei (15 to 30 0.2-mm slices/stack).

Focus quantification. Quantification of RAD-51 foci was performed for all seven zones composing the premeiotic tip to late pachytene regions of the germ line, as described in reference 42. The total numbers of nuclei scored per zone (arranged sequentially from zone 1 to zone 7) from three gonads from each genotype without irradiation was as follows: wild-type, 96, 120, 103, 84, 102, 60, and 56; *spo-11*, 127, 135, 117, 113, 114, 91, and 74; *mre-11(iow1)*, 159, 149, 115, 94, 84, 64, and 68; *cKu-80*, 81, 101, 88, 90, 87, 75, and 75; *mre-11(iow1)*; *cKu-80*, 133, 127, 104, 99, 51, 67, and 72; *exo-1*, 81, 117, 108, 88, 80, 64, and 60; *exo-1*; *cKu-80 [mre-11(iow1)/nT1]*; *exo-1*; *cKu80* were used as *exo-1*; *cKu-80* double mutants], 80, 84, 88, 62, 54, 52, and 46; *mre-11(iow1)*; *exo-1*, 58, 84, 96, 93, 75, 68, and 53; *mre-11(iow1)*; *exo-1*; *cKu-80*, 52, 60, 68, 68, 67, 61, and 50; *mre-11(ok179)*, 79, 110, 94, 88, 92, 89, and 71; *him-6*, 92, 110, 94, 74, 102, 71, and 60; *mre-11(iow1)*; *him-6*, 75, 84, 82, 77, 70, 71, and 56; and *mre-11(iow1)*; *him-6*; *cKu-80*, 75, 92, 93, 84, 83, 67, and 51. Due to the high number of RAD-51 foci per nucleus, only clearly nonoverlapped nuclei were counted from three gonads, except for *mre-11(iow1)*; *exo-1*. The total numbers of nuclei scored per zone (arranged sequentially from zone 1 to zone 7) from three gonads from each genotype with irradiation were as follows: wild-type, 58, 55, 40, 51, 47, 58, and 32; *spo-11*, 67, 50, 58, 55, 55, 38, and 38; *mre-11(iow1)*, 57, 90, 108, 108, 92, 73, and 66; *exo-1*, 69, 87, 69, 62, 55, 36, and 41; and *mre-11(iow1)*; *exo-1* (data from 6 gonads), 120, 175, 179, 154, 139, 124, and 109. Statistical comparisons between genotypes were performed using the two-tailed Mann-Whitney test, with 95% CI.

Quantification of RPA-1::YFP foci was performed in the same manner as for RAD-51 foci, with the following total numbers of nuclei scored per zone (arranged sequentially from zone 1 to zone 7) from the three gonads: *rpa-1::yfp*, 63, 73, 52, 55, 45, 38, and 39, and *mre-11(iow1)*; *rpa-1::yfp*, 51, 81, 76, 65, 61, 56, and 44. Statistical comparisons between genotypes were performed using the two-tailed Mann-Whitney test, with 95% CI.

Quantification of GFP::COSA-1 foci was performed for zone 8 and zone 9, composed of nuclei from late pachytene through diplotene, with the zone sizes as described in reference 42. The total numbers of nuclei scored for each type were as follows: *gfp::cosa-1*, 87 (3 gonads); *mre-11(ok179)*; *gfp::cosa-1*, 89 (4 gonads); *mre-11(iow1)*; *gfp::cosa-1*, 77 (3 gonads); *mre-11(iow1)/nT1*; *cKu-80*; *gfp::cosa-1*, 91 (5 gonads); *mre-11(iow1)*; *cKu-80*; *gfp::cosa-1*, 133 (5 gonads); *mre-11(iow1)/nT1*; *msh-5*;

TABLE 1 Embryonic lethality and HIM rate analysis

Genotype	Avg \pm SE no. of eggs laid (no. of broods)	% inviable eggs (total no. of eggs)	% males ^a (total no. of adults)
Wild type	217 \pm 43 (6)	0 (1,303)	0 (715)
<i>mre-11(ok179)</i>	156 \pm 23(8)	97.4 (1,247)	25 (12)
<i>mre-11(iow1)</i>	201 \pm 22 (3)	99.8 (605)	NA
<i>cKu-80</i>	178 \pm 43 (7)	0 (1,245)	0.4 (810)
<i>mre-11(ok179)/mre-11(iow1)</i>	213 \pm 37 (5)	99.9 (908)	NA
<i>mre-11(iow1); cKu-80</i>	163 \pm 77 (6)	87 (975)	16.7 (48)

^a The percentage of males was determined separately from embryonic lethality. NA, not applicable.

gfp::cosa-1, 78 (4 gonads); and *mre-11(iow1); msh-5; gfp::cosa-1*, 97 (3 gonads). Statistical comparisons between genotypes were performed using the two-tailed Mann-Whitney test, with 95% CI.

MRE-11 fluorescence intensity quantification. The fluorescence intensity of MRE-11 was quantified by using the ImageJ program. The fluorescence intensities (arbitrary signal intensity per area unit) of 12 nuclei and 12 cytoplasmic areas in the transition zone were measured per gonad and were normalized to the background intensity (arbitrary signal intensity per area unit). The quantification was done with the middle panel of the three-dimensional stacks, with a fluorescence threshold of 256, using ImageJ. The total number of nuclei and the cytoplasmic area scored for each type were as follows: wild type, 180 (15 gonads); *mre-11(ok179)*, 120 (10 gonads); and *mre-11(iow1)*, 60 (5 gonads). Statistical comparison between genotypes were performed using the two-tailed Mann-Whitney test, with 95% CI.

RESULTS

***mre-11(iow1)* is a hypomorph of *mre-11* with defects downstream of meiotic DSB formation.** *mre-11(iow1)* was isolated from a forward genetic screen (see Materials and Methods) designed to identify meiotic genes involved in chiasmata formation. *mre-11(iow)* failed to complement the null deletion mutation of *mre-11*, *mre-11(ok179)*, indicating *iow1* is allelic to *mre-11* (Table 1) (36). Sequencing of *mre-11(iow1)* revealed a C-T transition, expected to result in substitution of threonine (T) with isoleucine (I) at amino acid 72 (Fig. 1A and B). This threonine residue is conserved in all Mre-11 orthologs excluding that in *S. pombe* (Fig. 1B) and is located in the first phosphoesterase motif immediately upstream of the residue corresponding to D16 in *S. cerevisiae* (Fig. 1A and B). The D16 mutation causes a separation-of-function phenotype in *S. cerevisiae*; studies of the D16 mutation in *S. cerevisiae* have demonstrated that the first phosphoesterase motif is essential for the nuclease activity of Mre-11 (among other phenotypes [14, 41]).

We analyzed the morphology of meiotic chromosomes by staining DNA with DAPI (DAPI bodies). DSBs are generated when nuclei enter meiosis (transition zone) and are processed to form COs by late pachytene (42). However, these COs (chiasmata) cannot be observed cytologically until the diakinesis stage, when chromosomes are highly condensed. In *C. elegans*, the six pairs of homologous chromosomes (bivalents) are visualized as six DAPI bodies most clearly in diakinesis 1 (at the last oocyte stage before fertilization) (Fig. 1C). A complete loss of crossovers results in 12 DAPI bodies, each representing one univalent (one chromosome, e.g., *spo-11* [38]). Defects in the repair of DSBs lead to a different outcome; DAPI bodies of varied sizes and numbers between 1 and >12 are observed (e.g., *rad-51*, *com-1*, and *Cebrc-2*

[34, 39, 40]). We considered DAPI bodies as those that by visual inspection appeared smaller than the size of a univalent as fragments, while ones that appeared bigger than a bivalent were considered aggregates. We reasoned that oocytes with fewer than six DAPI bodies must have at least one aggregate. The *mre-11(iow1)* mutants showed a combination of chromosomal aggregates and fragments (which ranged from 1 to 14), sharply contrasting with the 6 bivalents or 12 univalents observed in the wild type and the null *mre-11(ok179)* mutant, respectively (Fig. 1C, D, and E). The 12 univalents observed in *mre-11(ok179)* mutants indicated a great reduction in meiotic DSB formation, while the aggregates and fragments of *mre-11(iow1)* mutants also have been found in mutants that fail to repair meiotic DSBs via HR (e.g., *rad-51*, *com-1*, and *Cebrc-2* [34, 39, 40]). The *mre-11(iow1)* allele is recessive to the wild-type allele of *mre-11*, because the diakinesis oocytes of *mre-11(iow1)/+* worms contained six DAPI bodies (data not shown). The *mre-11(iow1)* allele failed to complement the null *mre-11(ok179)* allele, because oocytes of *mre-11(iow1)/mre-11(ok179)* mutants showed chromosomal aggregates and fragments, a phenotype similar to the *mre-11(iow1)* homozygous mutant (Fig. 1F). The observation that oocytes of *mre-11(iow1)/mre-11(ok179)* mutants were similar to *mre-11(iow1)* mutants strongly suggests that a residual function of MRE-11 is retained by the protein encoded by the *iow1* allele.

An inability to form bivalents leads to chromosome missegregation in meiosis I. Nondisjunction of the X chromosome in meiosis I results in an increased percentage of males (XO) with the HIM (high incidence of males) phenotype. Nondisjunction of autosomes leads to inviable aneuploid embryos (36, 43). Compared to the wild type, *mre-11(iow1)* and *mre-11(ok179)* mutants both showed elevated levels of embryonic lethality (Table 1) (Fisher's exact test, $P < 0.0001$). The embryonic lethality of *mre-11(iow1)* progeny was significantly higher than that of *mre-11(ok179)* progeny (Table 1) (Fisher's exact test, $P < 0.0001$), consistent with the severe defects of chromosomal morphology observed in oocytes of *mre-11(iow1)*. Most lethality of *mre-11(ok179)* progeny can be attributed to aneuploidy due to chromosome missegregation in meiosis (36). The even greater lethality of *mre-11(iow1)* progeny presumably reflects the combined consequences of missegregation and defective repair of meiotic DSBs. The almost-complete embryonic lethality has also been observed in meiotic DSB repair mutants (e.g., *rad-51*, *com-1*, and *Cebrc-2* [34, 39, 40]). The embryonic lethality of *mre-11(iow1)/mre-11(ok179)* progeny was indistinguishable from that of *mre-11(iow1)* progeny, in agreement with the dominance of the *mre-11(iow1)* allele over that of the null *mre-11(ok179)* allele (Table 1) (Fisher's exact test, $P = 1$). The embryonic lethality analysis and cytological examination both suggested that *mre-11(iow1)* is a hypomorph of *mre-11* with defects downstream of meiotic DSB formation.

The defects observed in *mre-11(iow1)* mutants could be attributed to a reduction in the level of the MRE-11 protein. Alternatively, they could be due to specific perturbation of one of the activities of MRE-11, while retaining others (separation of function). To test whether protein levels of MRE-11 were affected by the *mre-11(iow1)* missense mutation, we performed Western blotting and immunohistochemical analysis using a *C. elegans* MRE-11-specific antibody. Western blot analysis of MRE-11 revealed an ~90-kDa band in protein extracts from wild-type worms, as previously found (see Fig. S1 in the supplemental material) (44). This band was absent from the null

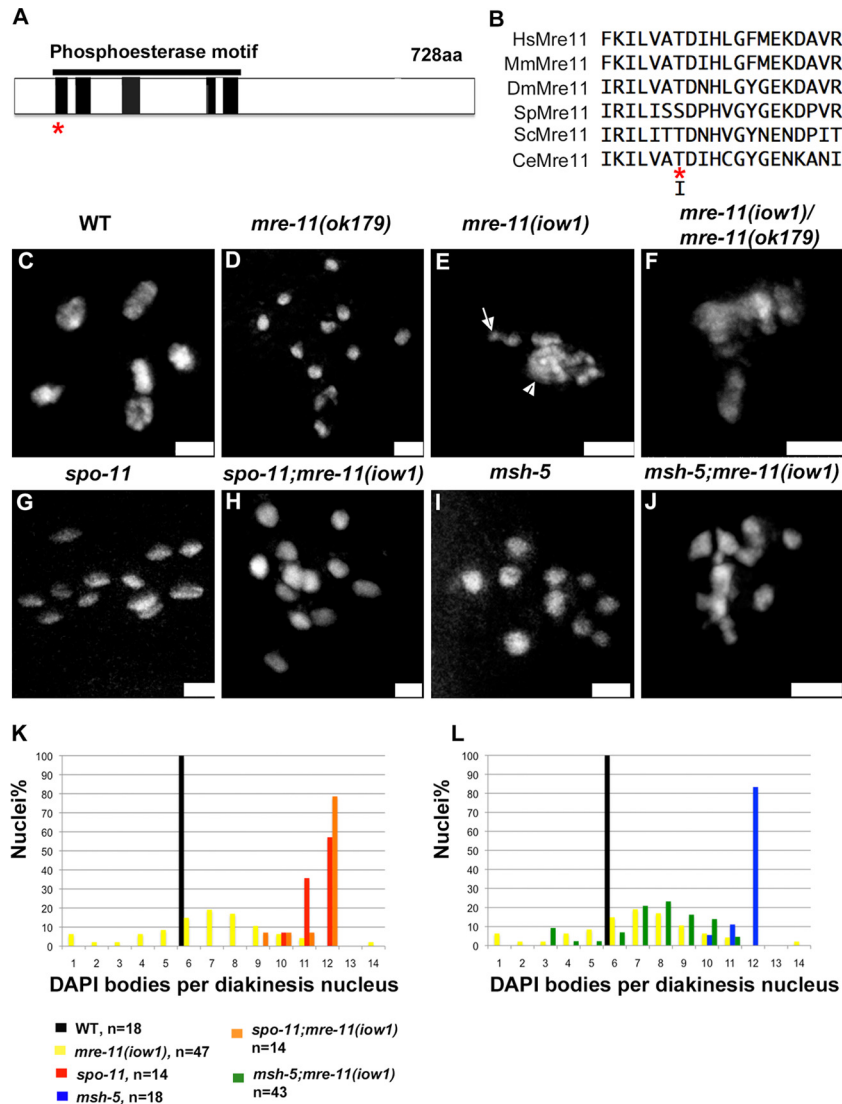


FIG 1 Defects in DSB repair in the *mre-11(iow1)* mutant. (A) Protein architecture of the predicted *C. elegans* MRE-11 protein. Black segments indicate the five conserved phosphoesterase motifs (14). The asterisk marks the point mutation in *mre-11(iow1)*. (B) *C. elegans* MRE-11 predicted protein sequence of the first phosphoesterase motif, aligned with orthologs from human, mouse, *Drosophila melanogaster*, *S. pombe*, and *S. cerevisiae*. The asterisk marks the point mutation of *mre-11(iow1)*. (C to J) Single DAPI-stained oocyte nuclei of the indicated genotypes at diakinesis I. Each panel shows a projection of a three-dimensional stack of the entire nucleus. The arrowhead indicates a chromosomal aggregate, and the arrow indicates chromosomal fragments. Bars, 2 μ m. (K and L) Frequency distribution of DAPI bodies at diakinesis I.

mre-11(ok179) mutants but still present in similar levels in *mre-11(iow1)* mutants, indicating that the *iow1* mutation does not affect the levels of the MRE-11 protein. The same antibody localized to germ line nuclei as multiple foci in wild-type worms (see Fig. S1D to F and J) (44). The nuclear localization, but not the cytoplasmic staining, was mostly absent in the *mre-11(ok179)* null mutant (see Fig. S1A to C and J), indicating that the nuclear localization is specific to MRE-11. MRE-11 nuclear foci were abundant in the germ line of *mre-11(iow1)* mutants (see Fig. S1G to J), consistent with the protein level of MRE-11 not being affected in *mre-11(iow1)* mutants. These data support the hypothesis that the meiotic defects of *mre-11(iow1)* mutants are due to perturbation of the resection activity of the MRE-11 protein and not due to the transcription, translation, and/or protein stability of MRE-11.

Recombination intermediates fail to form in *mre-11(iow1)* mutants. The resection activity of Mre11 is required to resect meiotic DSBs, which generate ssDNA, promoting subsequent repair by the HR pathway to yield crossovers in yeast (10–13). If the *C. elegans mre-11(iow1)* mutants are proficient in DSB formation but not in repair due to the perturbation of resection activity, we would expect that *spo-11* (required for DSB formation) would be epistatic to *mre-11(iow1)* (34, 40). In *spo-11* null mutants, DSBs were not formed and no crossovers were present, resulting in 12 univalents (Fig. 1G) (38). A *spo-11* mutation suppressed the aggregation and fragmentation phenotypes observed in *mre-11(iow1)* mutants; oocytes from *mre-11(iow1)*; *spo-11* double mutants displayed a majority of nuclei with 11 or 12 DAPI bodies (Fig. 1H and K). This result was not significantly different from that for *spo-11* single mutants (two-tailed Mann-Whitney test,

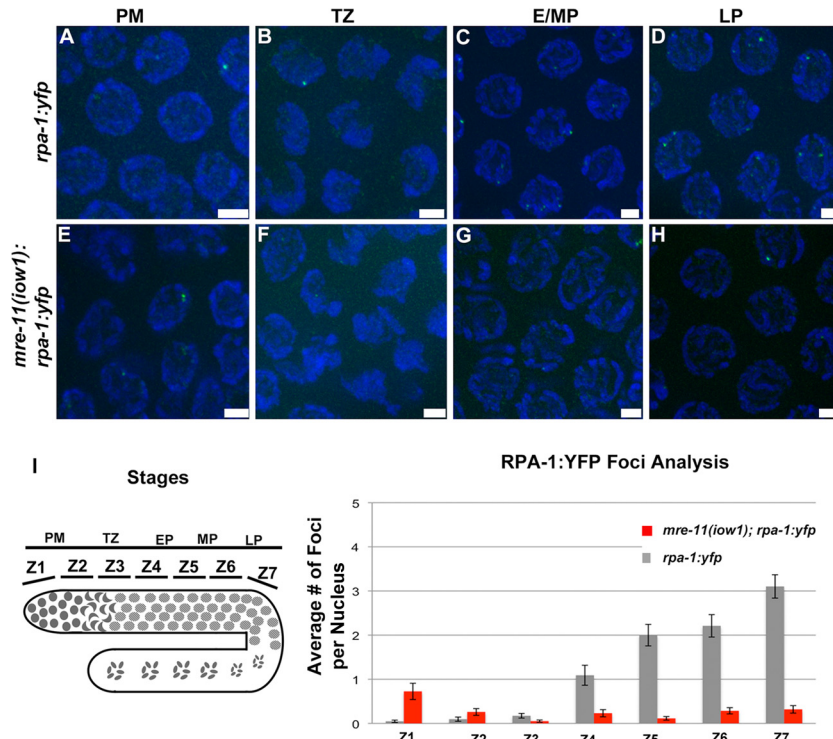


FIG 2 Lack of RPA-1 foci in *mre-11(iow1)* mutants. (A to H) Micrographs of YFP-tagged RPA-1 foci in the nuclei of indicated stages and indicated genotypes. Images are projections through three-dimensional data stacks. RPA-1::YFP foci are shown in green, and DAPI-stained chromosomes are shown in blue. Bar, 2 μ m. (I) Graph of a gonad, representing division of 7 zones from the premeiotic tip to late pachytene. PM, premeiotic tip; TZ, transition zone; EP, early pachytene; MP, middle pachytene; LP, late pachytene. Quantitative time course analysis of RPA-1::YFP foci during meiotic prophase I. The position along the x axis corresponds to zones in the germ line.

$P = 0.48$) but was significantly different from that for *mre-11(iow1)* mutants (two-tailed Mann-Whitney test, $P < 0.0001$). MSH-5 is a member of the ZMM proteins, which are needed to promote CO formation (45), and *C. elegans* MSH-5 functions after the formation of the RAD-51 nucleofilament but upstream of dHJ resolution (46). Diakinesis 1 oocytes of *msh-5* mutants showed 12 univalents due to defects in CO formation, while they retained the ability to repair DSBs through other homology-dependent pathways (Fig. 1I and L) (46). As expected, the *msh-5* mutation did not suppress the phenotype observed in *mre-11(iow1)* mutants. The number of DAPI bodies in oocytes of *mre-11(iow1); msh-5* double mutants showed a wide range of distribution, from 3 to 11 (Fig. 1J and L), sharply contrasting with the 12 univalents in the *msh-5* single mutants (Fig. 1I and L) (two-tailed Mann-Whitney test, $P < 0.0001$). Statistical analysis indicated a subtle but significant difference of DAPI body counts between the *mre-11(iow1); msh-5* double mutants and the *mre-11(iow1)* mutants (two-tailed Mann-Whitney test, $P = 0.037$). This could be due to some residual repair of DSBs via the HR pathway of *mre-11(iow1)*, which was eliminated by the *msh-5* mutation. All results taken together indicate that *mre-11(iow1)* acts downstream of DSB formation and upstream of CO formation, as expected for a mutant defective in DSB resection.

C. elegans meiotic chromosomes lack strong DSB hot spots (47, 48), and therefore, no molecular assays are available to determine the levels of DSB formation and resection. However, cytological markers for proteins associated with DSBs are extensively used for this purpose (34, 40). RPA-1 loads onto the newly generated

ssDNA concurrently with DSB resection. RPA-1 loading then facilitates the association of RAD-51 with the ssDNA (34), which forms a stable filament. To determine if ssDNA was generated in the germ line of *mre-11(iow1)* mutants, we measured the numbers of RPA-1 and RAD-51 foci in wild type, *mre-11(iow1)*, and *spo-11* mutants. Worm germ lines were divided into 7 zones (as described in reference 42) (Fig. 2I), and numbers of RPA-1 and RAD-51 foci were assessed in mitosis (zones 1 and 2), transition zone (zone 3), and pachytene (zone 4 to zone 7).

To test the hypothesis that resection is greatly reduced in *mre-11(iow1)* mutants, we examined the loading of yellow fluorescent protein (YFP)-tagged RPA-1 onto meiotic chromosomes of the wild type and *mre-11(iow1)* mutants. In the wild-type germ line, we observed an increase in the number of RPA-1 foci starting in early pachytene, eventually peaking at late pachytene (Fig. 2C, D, and I) (34). However, we did not observe an increased number of RPA-1 foci in pachytene in the *mre-11(iow1)* mutant germ line (Fig. 2G, H, and I). This is consistent with the hypothesis that resection is greatly reduced in the *mre-11(iow1)* mutant germ line.

We observed that the number of RAD-51 foci in the wild-type germ line rose upon entrance into the transition zone (Fig. 3A and 4B; see also Table S1 in the supplemental material), peaked at early-middle pachytene (Fig. 3A' and 4B; see also Table S1), and were mostly absent by late pachytene (Fig. 3A'' and 4B; see also Table S1), as previously demonstrated (42). The number of RAD-51 foci was low through the germ line of *spo-11* mutants (Fig. 3B and 4C; see also Table S1) due to absence of meiotic DSBs (38). The number of RAD-51 foci in the *mre-*

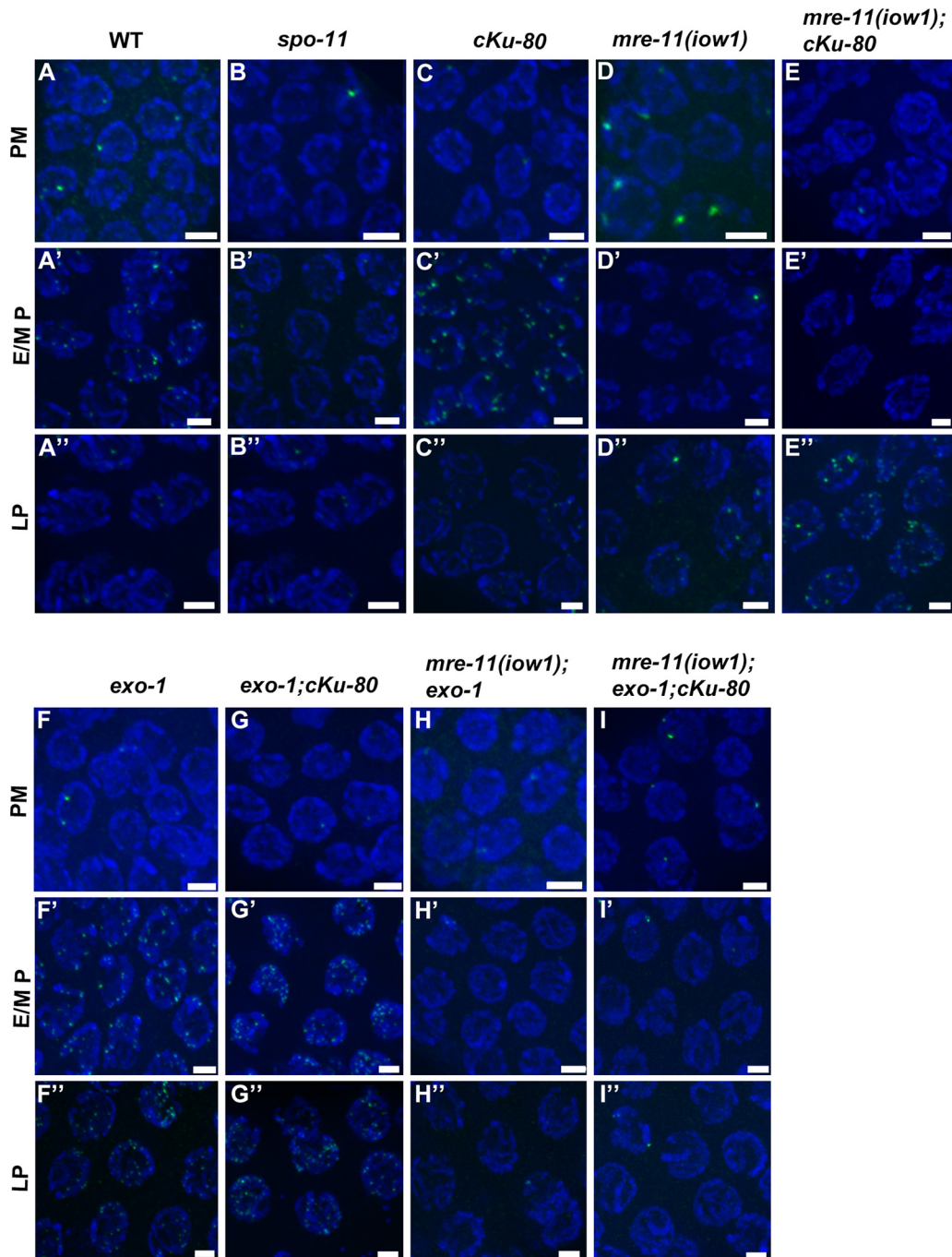


FIG 3 RAD-51 foci at meiotic prophase I in germ lines of different mutants. Immunofluorescence micrographs show RAD-51 foci of germ line nuclei of the indicated genotypes. PM, premeiotic tip; E/M P, early-middle pachytene; LP, late pachytene. Images are projections through three-dimensional data stacks. RAD-51 foci are shown in green, and DAPI-stained chromosomes are shown in blue. Bar, 2 μ m.

11(iow1) mutant germ line remained low from the transition zone to late pachytene, with most nuclei exhibiting no RAD-51 foci (Fig. 3D and 4E; see also Table S1), similar to what was observed in *spo-11* controls.

Crossover formation is greatly reduced in the *mre-11(iow1)* mutant germ line. COSA-1, a cyclin-related protein conserved in metazoans, is required for meiotic COs and localizes to the single CO site in each homolog in late prophase I (49). We tested

whether CO formation was defective in the germ line of *mre-11(iow1)* mutants by examining the loading of green fluorescent protein (GFP)-tagged COSA-1 onto meiotic chromosomes in wild-type, *mre-11(ok179)*, and *mre-11(iow1)* worms. The average number of COSA-1 foci for wild-type worm nuclei (from pachytene through diplotene) was 5.95 ± 0.04 (average \pm standard error [SE]), with most nuclei showing 6 bright COSA-1 foci corresponding to the 6 CO sites per nucleus (Fig. 5A, A', and F)

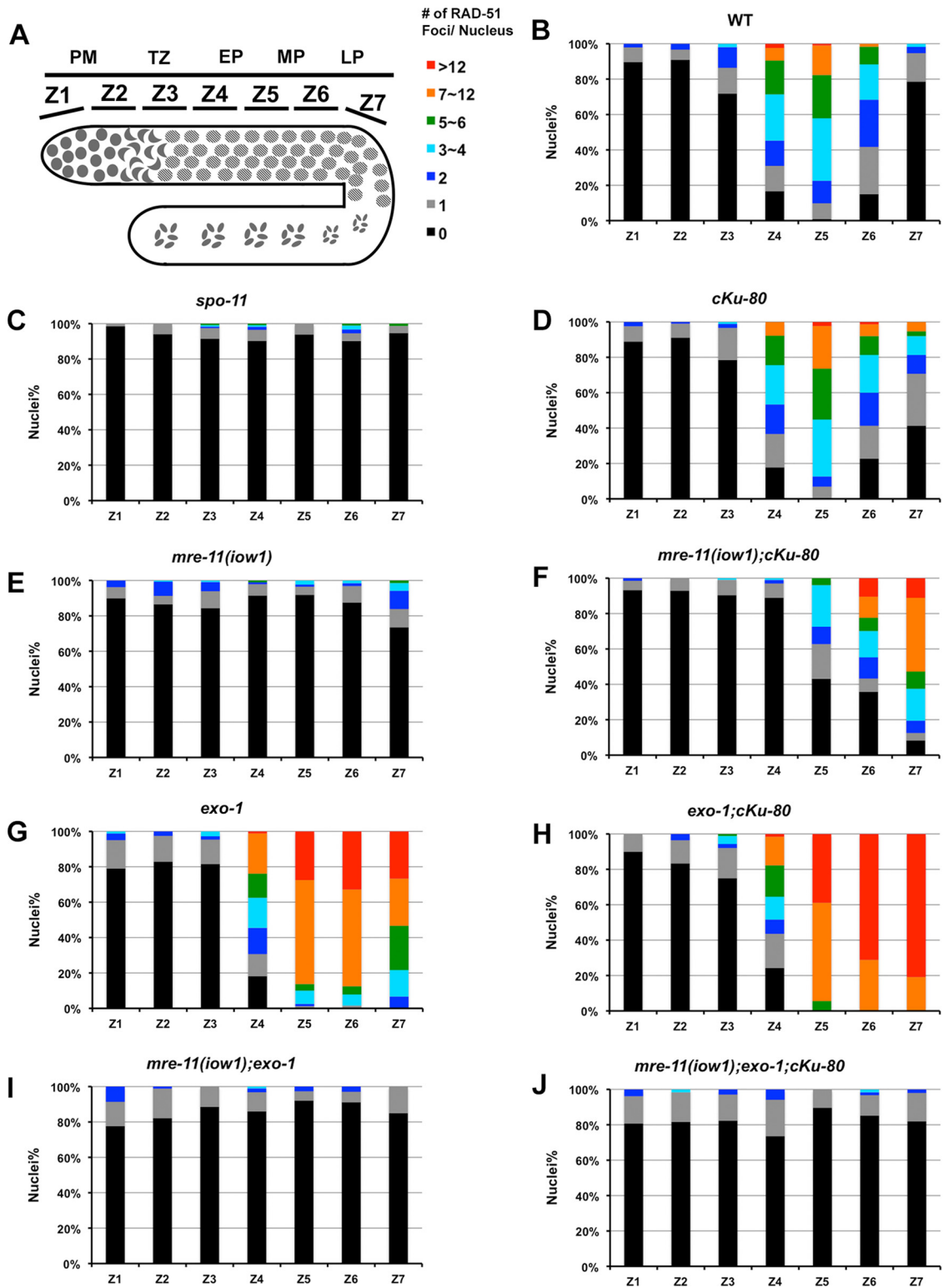


FIG 4 Quantitative time course analysis of RAD-51 foci at meiotic prophase I. (A) Graph of a gonad, representing division of the 7 zones from the premeiotic tip to late pachytene. PM, premeiotic tip; TZ, transition zone; EP, early pachytene; MP, middle pachytene; LP, late pachytene. (B to J) Levels of RAD-51 foci are indicated by color coding, as indicated to the left of panel B, showing the quantification of RAD-51 foci in the germ line of the indicated genotypes. The positions along the x axes correspond to zones in the germ line. The percentage of nuclei falling into each color-coded category is indicated on the y axes.

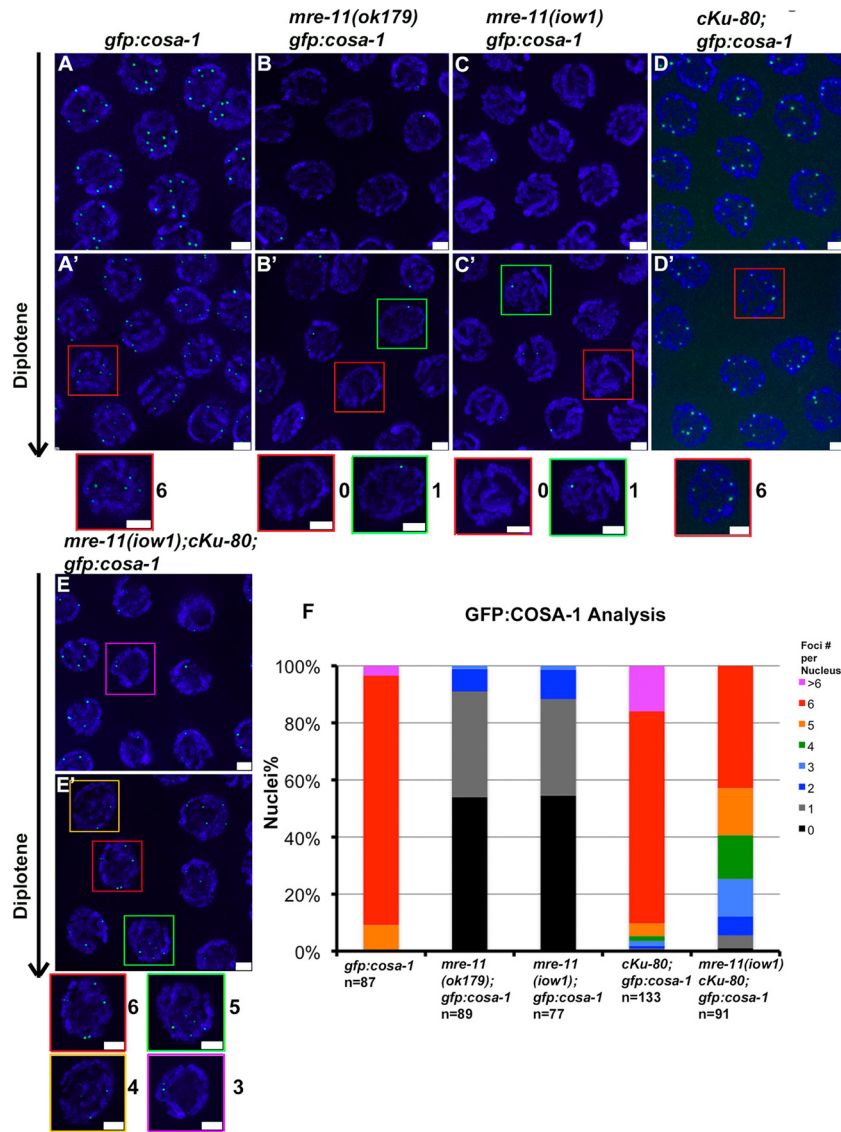


FIG 5 COSA-1 loading is reduced in the *mre-11(iow1)* mutant germ line but partially restored in *mre-11(iow1); cKu-80* mutants. (A to E) Immunofluorescence micrographs of GFP::COSA-1 foci of germ line nuclei of the indicated genotypes. Images are projections through three-dimensional data stacks. GFP::COSA-1 foci are shown in green, and DAPI-stained chromosomes are shown in blue. Bar, 2 μ m. (F) Quantitative analysis of GFP::COSA-1 foci observed in the different worms.

(49). In the *mre-11(ok179)* null mutant germ line at the same stages, the average number of foci per nucleus was 0.56 ± 0.07 (average \pm SE) (Fig. 5B, B', and F). In *mre-11(iow1)* mutants, the number of average foci per nucleus was 0.58 ± 0.08 (Fig. 5C, C', and F). These numbers were significantly lower than for the wild type (two-tailed Mann-Whitney test, $P < 0.0001$), but the results were indistinguishable from *mre-11(ok179)* mutants (two-tailed Mann-Whitney test, $P = 1$). This indicates that CO formation is severely reduced in *mre-11(iow1)* mutants.

To examine if the residual COSA-1 foci in *mre-11(iow1)* mutants resulted from repair of a few DSBs via HR, we examined if the absence of MSH-5 could eliminate those COSA-1 foci in *mre-11(iow1)* mutants. The average number of COSA-1 foci per nucleus for *mre-11(iow1); msh-5* mutants was 0.06 ± 0.02 (see Fig. S3C and D in the supplemental material), significantly lower than

in the *mre-11(iow1)* mutants (0.56 ± 0.07) (Fig. 5C and F) (two-tailed Mann-Whitney test, $P < 0.0001$), but indistinguishable from *msh-5* mutants (see Fig. S3A and D) (two-tailed Mann-Whitney test, $P = 0.85$). This elimination of the residual COSA-1 foci by the removal of MSH-5 in *mre-11(iow1)* mutants indicates that there is a small amount of HR-mediated repair in *mre-11(iow1)* mutants.

The absence of NHEJ partially suppresses the meiotic defects of *mre-11(iow1)* mutants. The chromosome aggregation observed in the oocytes of *mre-11(iow1)* mutants could be explained by repair of unresected meiotic DSBs via NHEJ. In the *C. elegans* germ line, it has been shown that some meiotic DSBs are repaired via NHEJ when HR is defective (e.g., *Cebrc-2* [34]). Therefore, we tested the hypothesis that DSB repair via NHEJ in the *mre-11(iow1)* mutant accounts for the chromosomal aggregates in this

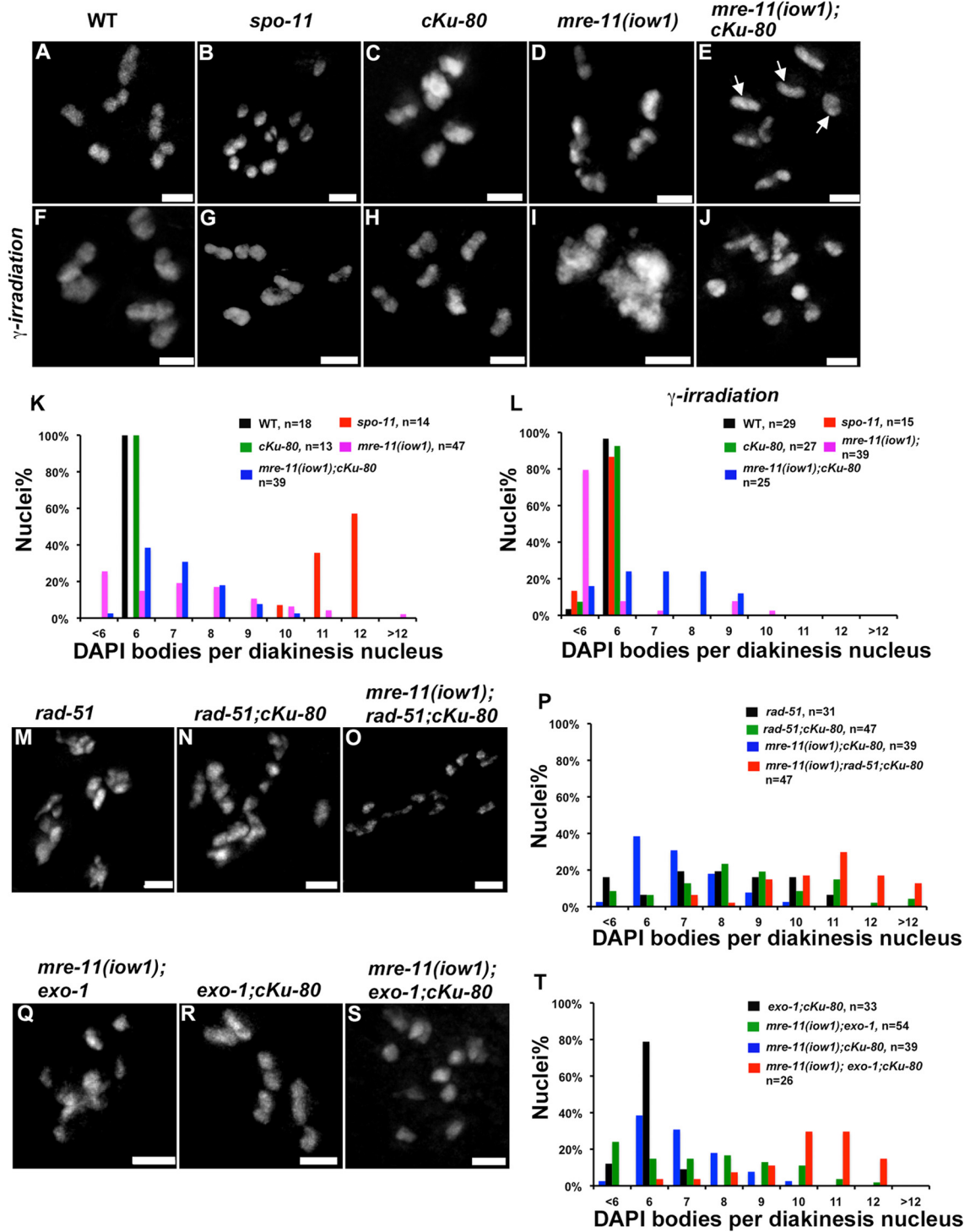


FIG 6 Chiasmata are partially restored in *mre-11(iow1); cKu-80* mutants but eliminated by depletion of RAD-51 and EXO-1. (A to E, M to O, and Q to S) DAPI-stained nuclei oocytes at diakinesis 1 of the indicated genotype. In the *mre-11(iow1); cKu-80* double mutant (E), bivalent-like DAPI bodies were observed (arrows). (F to J) DAPI-stained nuclei oocytes at diakinesis 1 post-gamma irradiation of the indicated genotypes. Bars, 2 μ m. (K, L, P, and T) Frequency distributions of DAPI-stained oocyte nuclei at diakinesis 1 under the indicated conditions.

mutant by creating double mutants of *mre-11; cKu-80*. *cKu-80* is the worm ortholog of Ku80 and is essential for NHEJ-mediated DSB repair (33). If some meiotic DSBs were acted on by NHEJ in *mre-11(iow1)* mutants, we would expect that removal of NHEJ by

a *cKu-80* mutation would suppress the chromosome aggregation in *mre-11(iow1)* mutants. The diakinesis 1 oocytes of *cKu-80* mutants showed 6 DAPI bodies, indistinguishable from the wild type (Fig. 6A, C, and K). This argues that the *C. elegans* germ line with

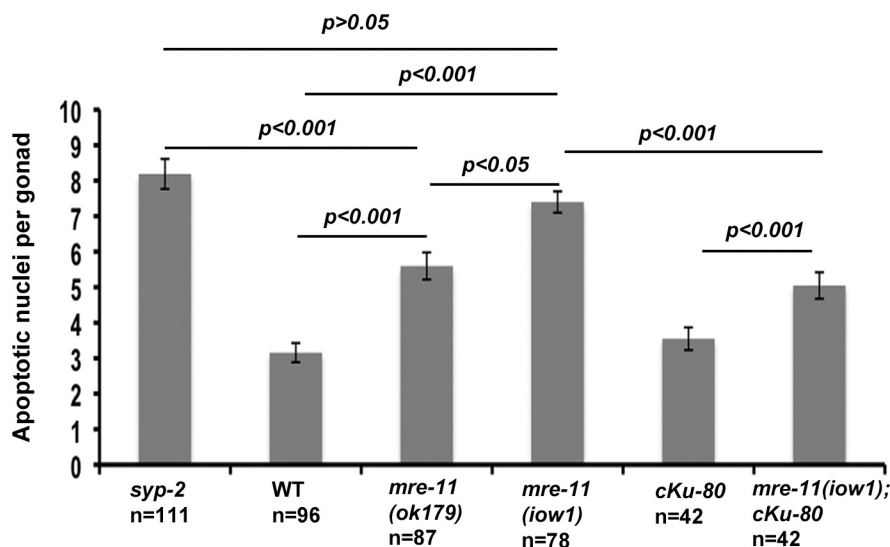


FIG 7 Germ line apoptosis is elevated in *mre-11(iow1)* mutants and is partially suppressed by blocking NHEJ. Acridine orange-stained apoptotic germ line nuclei were scored.

functional HR does not use NHEJ (33). The frequency of oocytes with aggregates in *mre-11(iow1); cKu-80* double mutants was significantly lower than oocytes of *mre-11(iow1)* single mutants, and some DAPI bodies in the oocytes of the double mutants appeared to be bivalent (Fig. 6E and K) (Fisher's exact test, $P < 0.01$). These data suggest that removal of *cKu-80* partially suppresses the chromosome aggregation contained by *mre-11(iow1)* mutants and supports our hypothesis that some chromosome aggregation in *mre-11(iow1)* mutants is due to the repair of meiotic DSBs via NHEJ.

The high level of embryonic lethality in *mre-11(iow1)* mutants is partially suppressed by the removal of NHEJ. To examine in more detail the effect of NHEJ removal on *mre-11(iow1)* mutants, we compared embryonic lethality and the HIM rate in the double mutants, single mutants, and wild-type worms. Compared to the single *mre-11(iow1)* mutants, the double mutant *mre-11(iow1); cKu-80* showed a significant decrease in embryonic lethality; 13.0% of the double mutant embryos laid hatched (Table 1) (Fisher's exact test, $P < 0.0001$), consistent with partial rescue in chromosomal aggregation in late prophase I. Among those hatched F1 progeny of *mre-11(iow1); cKu-80* mutants, the percentage of males was significantly higher than that of wild-type and *cKu-80* worms (Table 1) (Fisher's exact test, $P < 0.0001$), indicating defects in chromosome segregation.

The *cKu-80* mutation reduces the high level of germ line apoptosis in *mre-11(iow1)* mutants. In *C. elegans*, most recombination-defective mutants that exhibit chromosome aggregates and fragments in late prophase I also show a high level of apoptosis at late pachytene that is triggered by the DNA damage checkpoint (e.g., *rad-51* and *Cebr-2* [34, 50]). Since *mre-11(iow1)* mutants showed chromosome aggregates and fragments at late prophase I, we investigated whether germ line apoptosis was elevated in *mre-11(iow1)* mutants by staining germ line nuclei undergoing apoptosis with acridine orange (46). We found a 2-fold increase in the level of apoptotic nuclei in late pachytene of *mre-11(iow1)* mutants compared to the wild-type worms (Fig. 7) (two-tailed Mann-Whitney test, $P < 0.001$). Since removal of NHEJ partially suppressed the chromosome aggregates in *mre-11(iow1)* mutants,

we asked if removal of NHEJ would also suppress the high level of germ line apoptosis in *mre-11(iow1)* mutants. The levels of apoptosis in *mre-11(iow1); cKu-80* double mutants (Fig. 7) were significantly lower than those of *mre-11(iow1)* single mutants (Fig. 7) (two-tailed Mann-Whitney test, $P < 0.0001$) but significantly higher than in wild-type and *cKu-80* worms (Fig. 7) (two-tailed Mann-Whitney test, $P < 0.001$). The intermediate level of apoptosis in *mre-11(iow1); cKu-80* double mutants was consistent with the partial rescue of chromosome morphology of oocytes at diakinesis in the absence of NHEJ.

DSBs are repaired via the HR-mediated pathway in the *mre-11(iow1); cKu-80* mutant germ line. A possible explanation for the partial suppression of the *mre-11(iow1)* mutant phenotypes by the *cKu-80* mutation is that, when NHEJ is not available, DSBs are repaired via the HR pathway. The HR pathway is completely dependent on RAD-51 in *C. elegans* (no DMC1 is present). We therefore examined if a *rad-51* null mutation would eliminate bivalent formation in the *mre-11; cKu-80* mutants. The *mre-11(iow1); rad-51; cKu-80* triple mutants showed a high level of chromosomal fragmentation by DAPI bodies count (Fig. 6O and P), significantly different from *mre-11(iow1); cKu-80* (Fig. 6E and K) (two-tailed Mann-Whitney test, $P < 0.0001$) and from *rad-51; cKu-80* (Fig. 6N and P) (two-tailed Mann-Whitney test, $P < 0.0001$). This supports our hypothesis that repair of DSBs in *mre-11; cKu-80* depends on HR.

To further analyze the repair of DSBs in *mre-11(iow1); cKu-80*, we analyzed RAD-51 localization in *mre-11(iow1); cKu-80* double mutants. In agreement with our hypothesis, we observed RAD-51 loading onto chromosomes in the double mutants (Fig. 3E and 4F; see also Table S1 in the supplemental material). Moreover, RAD-51 loading was delayed in *mre-11(iow1); cKu-80* worms compared to the wild-type and *cKu-80* worms, in agreement with late activation of the HR pathway. RAD-51 foci did not load onto chromosomes in the germ line of *mre-11(iow1); cKu-80* worms through early pachytene (Fig. 3E and E' and 4F; see also Table S1). RAD-51 foci started to increase around middle pachytene and peaked at late pachytene (Fig. 3E'' and 4F; see also Fig. S4B and Table S1 in the supplemental material). The number of RAD-51

foci on germ line chromosomes in late pachytene of *mre-11(iow1)*; *cKu-80* worms was significantly higher than the foci at the corresponding stage of wild-type, *mre-11(iow1)*, or *cKu-80* worms (Fig. 3 and 4; see also Fig. S4 and Table S1) (pairwise comparison of foci in zone 7, two-tailed Mann-Whitney test, $P < 0.0001$). The loading of RAD-51 in late meiotic prophase I in *mre-11(iow1)*; *cKu-80* worms suggests DSBs are resected in *mre-11(iow1)* mutants when NHEJ is not available for their repair, albeit in later stages than observed in the wild-type worms.

To further demonstrate that DSBs are repaired by the HR pathway to give rise to COs in *mre-11(iow1)*; *cKu-80* double mutants, we examined the loading of GFP-tagged COSA-1 onto the chromosomes in the double mutants. The number of COSA-1 foci per nucleus from late pachytene through diplotene in the germ line of *mre-11*; *cKu-80* double mutants was 4.58 ± 0.16 (average \pm SE) (Fig. 5E, E', and F). This COSA-1 foci level in *mre-11*; *cKu-80* double mutants was significantly higher than that of *mre-11(iow1)* single mutants (Fig. 5C and F) (two-tailed Mann-Whitney test, $P < 0.0001$) but significantly lower than *cKu-80* and wild-type worms (Fig. 5A, D, and F) (two-tailed Mann-Whitney test, $P < 0.0001$). The partial restoration in the COSA-1 loading in *mre-11(iow1)*; *cKu-80* double mutants suggests formation of COs in most nuclei and is consistent with the partial suppression of *mre-11(iow1)* by *cKu-80* mutation for other phenotypes.

The repair of DSBs in *mre-11(iow1)*; *cKu-80* mutant germ line requires EXO-1. The delayed loading of RAD-51 in the *mre-11(iow1)*; *cKu-80* mutant germ line can be interpreted as resection of meiotic DSBs by an alternative nuclease, which is active from middle to late prophase I. Exo1 and BLM (the orthologs in worms are EXO-1 and HIM-6) have been shown to be involved in resection activity in DSB ends in yeast (3, 4). To examine if Exo1 and BLM contribute to the repair of meiotic DSBs in *mre-11(iow1)*; *cKu-80* mutants, we constructed *mre-11(iow1)*; *exo-1*; *cKu-80* and *mre-11(iow1)*; *him-6*; *cKu-80* triple mutants.

Most diakinesis 1 oocytes of *exo-1*; *cKu-80* double mutants showed 6 DAPI bodies (Fig. 6R and T), a result indistinguishable from the wild type (Fig. 6A and K) (two-tailed Mann-Whitney test, $P = 0.87$) and *exo-1* worms (data not shown; two-tailed Mann-Whitney test, $P = 0.64$). The diakinesis 1 oocytes of *mre-11(iow1)*; *exo-1* mutants showed chromosomal aggregation and fragmentation (Fig. 6Q and T), similar to *mre-11(iow1)* mutants (Fig. 6D and K) (two-tailed Mann-Whitney test, $P = 1$). The majority of *mre-11(iow1)*; *exo-1*; *cKu-80* triple mutant oocytes showed 11 or 12 DAPI bodies (Fig. 6S and T), sharply contrasting with the *mre-11*; *cKu-80* mutants (Fig. 6E and K) (two-tailed Mann-Whitney test, $P < 0.0001$). This indicates that the repair of DSBs in *mre-11(iow1)*; *cKu-80* via HR is greatly reduced in the absence of *exo-1*.

We also examined if the absence of EXO-1 could eliminate or reduce the RAD-51 foci observed from middle to late prophase I in *mre-11(iow1)*; *cKu-80* mutants. The germ line of *exo-1* mutants exhibited wild-type loading patterns of RAD-51 (transition zone to late pachytene) (Fig. 3F and 4G; see also Table S1 in the supplemental material); however, it did not disappear in late pachytene (Fig. 3F' and 4G; see also Table S1). This indicated defects in dissolution of RAD-51 in the *exo-1* mutant germ line. The germ line of *exo-1*; *cKu-80* mutants showed a similar RAD-51 loading pattern as *exo-1* mutants (Fig. 3G and 4H; see also Table S1). The RAD-51 foci remained low throughout the germ line of *mre-11(iow1)*; *exo-1* mutants (Fig. 3H and 4I; see also Table S1), similar

to *mre-11(iow1)* mutants (Fig. 3D and 4E; see Table S1). Removal of *exo-1* in the *mre-11(iow1)*; *cKu-80* background eliminated RAD-51 loading through pachytene (Fig. 3E and I and 4F and J; see also Table S1) (pairwise comparison of foci in zone 6 and 7, two-tailed Mann-Whitney test, $P < 0.0001$). Overall, our data support a role for EXO-1 in the resection of DSBs from middle to late pachytene in *mre-11*; *cKu-80* mutants. Interestingly, we observed RAD-51 foci in nuclei in diplotene to diakinesis in *mre-11*; *exo-1*; *cKu-80* triple mutants (see Fig. S4C in the supplemental material), which indicates another resection activity independent of EXO-1 and MRE-11 in these very late stages of meiotic prophase I.

To examine the role of HIM-6 in resection, we quantitated the DAPI bodies and RAD-51 loading in *mre-11(iow1)*; *him-6*; *cKu-80* triple mutants. The majority of oocytes of *mre-11(iow1)*; *him-6*; *cKu-80* triple mutants showed 11 or 12 DAPI bodies (data not shown). However, the RAD-51 focus loading pattern of *mre-11(iow1)*; *him-6*; *cKu-80* was not different from that of *mre-11*; *cKu-80* mutants (Fig. 3E and 4F; see also Fig. S2D and H and Table S1 in the supplemental material). This indicates *him-6* does not contribute to resection in *mre-11(iow1)*; *cKu-80* mutants but has a role downstream of resection, as previously reported (51).

The repair of gamma irradiation-induced DSBs in *mre-11(iow1)* mutants depends on NHEJ and EXO-1. Unlike programmed meiotic DSBs, DSBs introduced by ionizing irradiation (IR) are not bound by Spo11. IR-induced DSBs can be repaired via the HR pathway to yield COs in the *C. elegans* germ line (37). Previous studies showed that null mutations of the MRX/N complex genes confer a profound defect in the response of germ cells to IR-induced DNA damage (36, 37). To test whether it is the resection activity of *mre-11* that is required in the IR-induced DNA damage response, we used gamma irradiation to examine the *mre-11(iow1)* mutants.

We examined chromosome morphology in diakinesis 1 oocytes 24 h post-gamma irradiation. Under these conditions, wild-type and *cKu-80* worms showed 6 DAPI bodies, comparable to their nonirradiated counterparts (Fig. 6A, F, C, H, K, and L). Irradiated *spo-11* mutants had 84% oocytes with 6 DAPI bodies (Fig. 6B, G, K, and L). This indicated that DSBs introduced under these experimental conditions were sufficient to restore chiasmata in *spo-11* mutants. The occurrence of oocytes with aggregates in irradiated *mre-11(iow1)* mutants was significantly higher than in the nonirradiated counterparts (Fig. 6D, I, K, and L) (Fisher's exact test, $P < 0.0001$). The occurrence of oocytes with aggregates in irradiated *mre-11(iow1)* mutants was significantly reduced by the *cKu-80* mutation (Fig. 6I, J, K, and L) (Fisher's exact test, $P < 0.0001$). Our data suggest that exogenous DSBs are repaired via NHEJ, resulting in severe chromosome aggregation in *mre-11(iow1)* mutants. This supports a requirement for functional MRE-11 to repair exogenous DSBs in the germ line. Interestingly, diakinesis oocytes of irradiated *mre-11(iow1)*; *cKu-80* double mutants did not show a significant difference in chromosomal morphology as measured by DAPI body counts compared to nonirradiated counterparts (Fig. 6E, J, K, and L) (two-tailed Mann-Whitney test, $P = 0.97$). This suggests efficient repair of exogenous DSBs in *mre-11(iow1)*; *cKu-80* double mutants by the HR pathway or an alternative pathway.

RAD-51 loading onto gamma-irradiated DSBs requires RAD-50 (and presumably MRE-11) in early to mid-meiotic prophase (transition zone to late pachytene), but it is dispensable for

late prophase nuclei and mitotically dividing nuclei (37). Thus, the *C. elegans* germ line switches between RAD-50/MRE-11-independent and -dependent loading of RAD-51 as cells enter meiosis. This is speculated to be due to a requirement for the resection of DSBs by the MRX/N complex only in early to midprophase. To investigate if the resection activity of MRE-11 was required for RAD-51 loading at DSBs sites generated by IR, we analyzed RAD-51 localization in gamma-irradiated *mre-11(iow1)* mutants. Germ line nuclei from mitosis to meiotic prophase I in irradiated wild-type and *spo-11* worms are capable of loading RAD-51 (Fig. 8A, B, F, and G; see also Table S1 in the supplemental material). In contrast with the wild-type and *spo-11* worms, RAD-51 foci were absent from the transition zone to mid- to late pachytene in irradiated *mre-11(iow1)* worms; their loading was reduced in the premeiotic zone and in late pachytene (Fig. 8A, B, D, F, G, and H; see also Table S1). Similar numbers of RAD-51 foci were also observed in *mre-11(ok179)* null mutants (see Fig. S5A in the supplemental material). The failure to accumulate RAD-51 from the onset of meiosis to midpachytene in irradiated *mre-11(iow1)* worms indicates MRE-11 is required to resect DSBs at these stages, supporting previous findings (37). As expected, *cKu-80* mutants were indistinguishable from the wild type in their response to IR, consistent with NHEJ being dispensable for germ line DSB repair in the presence of functional HR (see Fig. S5D). In agreement with our observation of the role of NHEJ in repair of meiotic DSBs under HR-defective conditions, irradiated *mre-11(iow1)*; *cKu-80* double mutants showed an increase in RAD-51 foci on exogenous DSBs in late prophase I compared to the irradiated *mre-11(iow1)* single mutants, but RAD-51 loading at earlier stages of meiosis was unaffected (Fig. 8D and H; see also Fig. S5E).

As RAD-51 focus levels were reduced but not abrogated in the premeiotic zone and in late pachytene in *mre-11(iow1)* mutants, we hypothesized that the resection activity of MRE-11 is dispensable in mitosis and in late prophase I due to the redundant resection activities of EXO-1 or HIM-6. To examine whether EXO-1 or HIM-6 plays a role in resection of irradiation-induced DSBs in *mre-11(iow1)* mutants, we analyzed RAD-51 loading in irradiated *mre-11(iow1)*; *exo-1* and *mre-11*; *him-6* double mutants. Compared to irradiated *mre-11(iow1)* mutants, irradiated *mre-11(iow1)*; *exo-1* worms showed greatly reduced RAD-51 foci in the premeiotic tip (Fig. 8D, E, H, and J; see also Table S1 in the supplemental material) (pairwise comparison of foci in zones 1 and 2, two-tailed Mann-Whitney test, $P < 0.0001$) and showed elimination of RAD-51 foci in late pachytene (Fig. 8D', E', H, and J; see also Table S1) (pairwise comparison of foci in zone 7, two-tailed Mann-Whitney test, $P < 0.0001$). Nevertheless, removal of HIM-6 in *mre-11(iow1)* mutants did not result in a reduction in the premeiotic tip and late pachytene (see Fig. S5B and C in the supplemental material). These results indicated that EXO-1 is responsible for the resection of irradiation-induced DSBs in late pachytene when MRE-11's resection activity is impaired.

DISCUSSION

A conserved function for the nuclease domain of MRE-11 in DSB resection. Here we identified the first separation-of-function allele of the MRX/N complex in *C. elegans* and provided clear evidence of a role for MRE-11 in the resection of meiotic, SPO-11-induced DSBs in *C. elegans*. Several lines of evidence indicated that *iow1* mutation affects resection rather than DSB formation:

(i) *mre-11(iow1)* meiotic defects appeared downstream of DSB formation; (ii) *spo-11* deletion was able to suppress the chromosomal abnormalities of *mre-11(iow1)* mutants; (iii) elimination of NHEJ in *mre-11(iow1)* mutants largely restored RAD-51 loading and CO formation. Meiotic DSBs cannot be properly repaired in the *mre-11(iow1)* mutant, and DSBs are likely not efficiently resected, as evidenced by defects in the loading of RPA-1 and RAD-51. The *mre-11(iow1)* mutant harbors a point mutation in the N-terminal phosphodiesterase domain, a domain found to be required for the nuclease activity of Mre11 in other species (10, 14–16). Specifically, the yeast “nuclease dead” separation-of-function allele Mre11-D16A/N mutation is in the same phosphodiesterase motif as the *iow1* mutation (14), suggesting that the nuclease activity of MRE-11 is affected in *C. elegans mre-11(iow1)* mutants. While we were unable to directly test whether *mre-11(iow1)* nuclease activity was completely abrogated when we used biochemical approaches, our data clearly argue for a conserved function for MRE-11 in meiotic DSB resection in metazoan meiosis.

The *mre-11(iow1)* mutation is most similar to the *S. cerevisiae* Mre11-D16A and Mre11-D16N mutations, which exhibit compromised MRX/N complex formation (as well as DNA damage sensitivity and telomere length defects [41]). Therefore, it is possible that MRX/N activity in the *mre-11(iow1)* mutant is affected due to compromised complex stability. The observation that MRE-11 foci are bigger and preferentially enriched in the chromosome of transition zone nuclei in wild-type worms but smaller and evenly distributed between chromosome and cytosol in *mre-11(iow1)* mutants could be a manifestation of compromised MRX/N stability. Alternatively, this may be explained by disruption of DNA binding activity of the complex. Although we were not able to test complex stability directly in the *mre-11(iow1)* mutant in the present study, the evidence indicates that the MRX/N complex assembles in *mre-11(iow1)* mutants: meiotic DSBs (which in *C. elegans* are dependent on the MRX/N complex [36, 37]) are formed at normal levels in *mre-11(iow1)* mutants. Additionally, the level of the MRE-11 protein in *mre-11(iow)* mutants is similar to that found in the wild type, suggesting that there is no aberrant turnover of the mutant protein. Whether the *mre-11(iow1)* mutation affects complex stability or not, the biological outcome is a separation of function of the two key activities, DSB formation and resection, of the MRX/N complex.

DSB repair pathway choice in the *C. elegans* germ line. NHEJ and HR are the two major pathways used to repair DSBs in most organisms (29). Results in *S. cerevisiae* and *S. pombe* have indicated that initiation of resection by MRX/N and Com1/Sae2 at mitotic DSB ends is critical to promote HR repair by dissociating KU from those ends (52–54). A recent report implied a role for COM-1 in antagonizing KU, preventing meiotic DSB repair via NHEJ in the *C. elegans* germ line (55). Prior to our work, it was unknown whether MRE-11 is required for antagonizing NHEJ in *C. elegans*. Our data suggest that MRE-11 is a critical component in committing repair of germ line DSBs to the HR pathway, as opposed to NHEJ, because the latter is used to repair both meiotic and irradiation-induced DSBs in the absence of a functional MRX/N. Repair of meiotic DSBs in *mre-11(iow1)* mutants via NHEJ indicated that SPO-11 is removed from DSB ends, because KU cannot act on DSB ends bound by SPO-11. The removal of SPO-11 from meiotic DSB ends in *mre-11(iow1)* mutants can be explained by

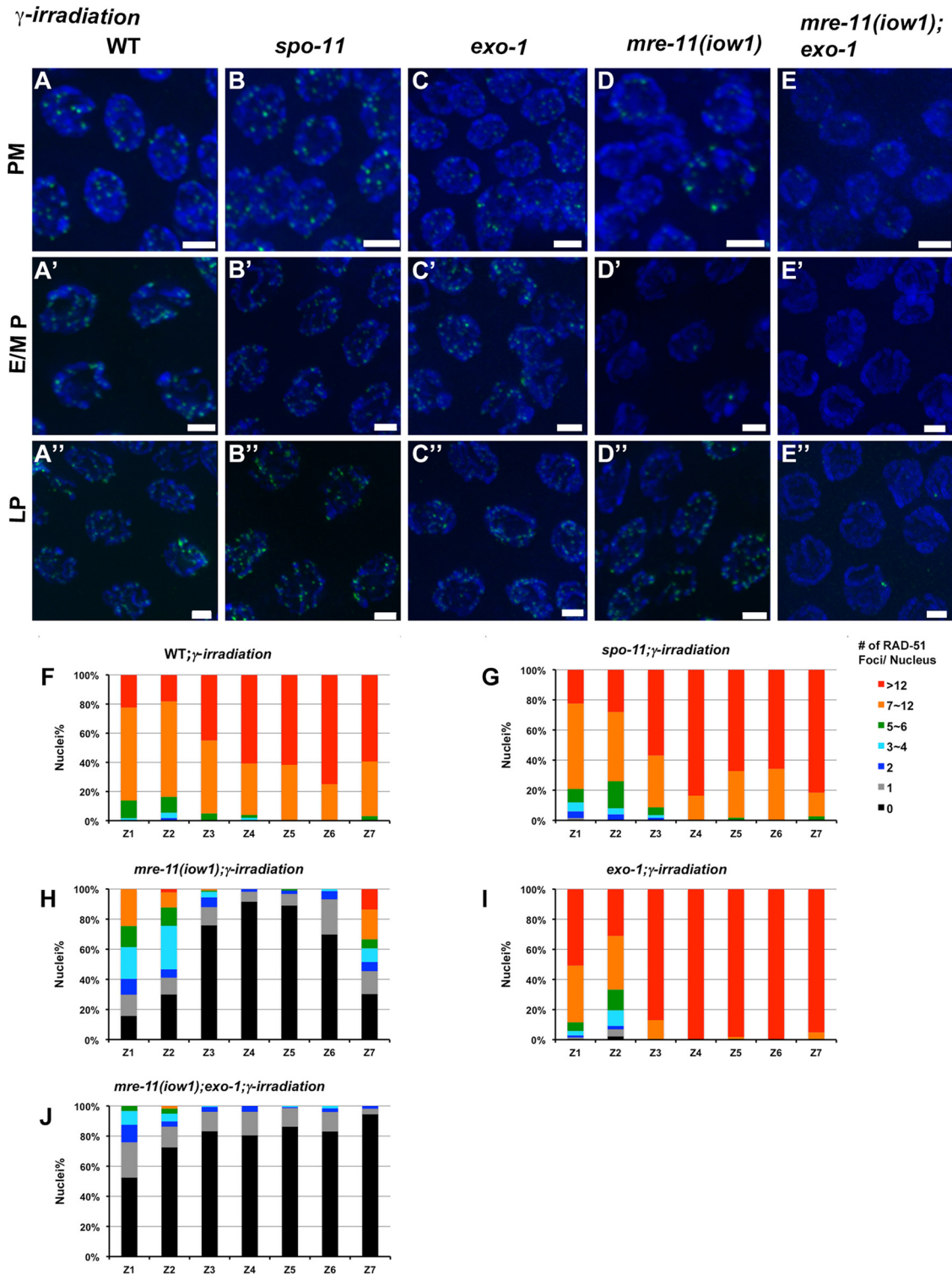


FIG 8 RAD-51 foci at meiotic prophase I in germ lines following gamma irradiation. (A to E) Immunofluorescence micrographs of RAD-51 foci of germ line nuclei following irradiation. PM, premeiotic tip; E/M P, early-middle pachytene; LP, late pachytene. Images are projections through three-dimensional stacks. RAD-51 foci are shown in green, and DAPI-stained chromosomes are shown in blue. Bar, 2 μ m. (F to J) Histograms showing quantification of RAD-51 foci in the germ line of the indicated genotypes. Positions along the x axes correspond to zones in the germ line. The percentage of nuclei falling into each color-coded category is indicated on the y axes.

a redundant resection activity of COM-1 (see Fig. S6 in the supplemental material). An alternative explanation would be that *mre-11(iow1)* has some residual nuclease activity that is sufficient for SPO-11 removal but not for generation of a sufficient amount of ssDNA that can be cytologically observed (RAD-51 and RPA-1 binding). Even though we do not yet possess the tools to test these two possibilities in *C. elegans*, our data still suggest a role for MRX/N in channeling repair of germ line DSBs to HR, which is critical for the maintenance of genomic integrity.

Alternative pathways for DSB resection in *C. elegans*. Work in yeast has indicated that meiotic DSB resection is initiated by Mre11 and Com1/Sae2 to generate short ssDNA that can be extensively resected by two resection activities: those of EXO-1 and Blm1/Sgs1-Dna2 (3, 4, 10, 14–16, 19, 56, 57). In a wild-type background, EXO-1 is not required for CO formation (this study and reference 55). In the MRE-11/RAD-50 null mutants, meiotic DSBs and therefore COs don't form. Thus, the position of EXO-1 in the pathway cannot be assessed. Our separation-of-function allele provides such an opportunity and uncovers a role for EXO-1 in resecting meiotic DSBs when MRX/N is not functional and NHEJ is blocked. Similarly, in the absence of COM-1 and NHEJ, EXO-1-dependent HR repair can restore CO formation, indicating a role for EXO-1 in the resection of meiotic DSBs when COM-1 is absent (55). However, the effects of EXO-1 depletion are different in worms deficient in a functional MRX/N and of COM-1; the deletion of EXO-1 can abrogate a larger fraction of COs in the *com-1*; *cKu-80* mutants compared to the *mre-11(iow1)*; *cKu-80* mutants. This implies that the resection activity of EXO-1 is independent of COM-1 but partially dependent on a functional MRX/N complex. Another interesting feature of EXO-1-dependent DSB resection is its different temporal activation (based on the RAD-51 focus kinetics) in backgrounds deficient in COM-1 (and NHEJ) and MRX/N (and NHEJ). In *com-1*; *cKu-80* worms, RAD-51 foci start to appear during early pachytene, similar to the pattern that is observed in the wild type (55). Depletion of EXO-1 in *com-1*; *cKu-80* mutants eliminates RAD-51 foci beginning in early pachytene. However, in *mre-11(iow1)*; *cKu-80* worms, RAD-51 foci do not start to appear until midpachytene. These results indicate that the resection activity of EXO-1 is dependent on a functional MRX/N only in early prophase I but not in later stages. We propose two explanations for this temporal dependence on MRX/N: (i) the impaired MRX/N resection activity reduces the amount of DNA substrates that EXO-1 can act on, and therefore EXO-1-dependent resection occurs slowly and RAD-51 does not load until midpachytene; or (ii) MRX/N can stimulate EXO-1's activity directly in early prophase I, independently from its effect on ssDNA formation. We prefer the second argument, because this is consistent with the physical interaction between Mre11 and Sgs1, and with a role for MRX/N in stimulating Sgs-Exo-1-mediated DSB end resection *in vitro* (56, 58, 59). Furthermore, when MRX/N is absent, EXO-1 still cannot act on free DSB ends produced by ionizing irradiation in early prophase I (zones 3 to 6 [this study and reference 37]). This supports a role for MRX/N in stimulating EXO-1 independently of its resection activity. Here, we propose that in *C. elegans*, MRX/N is required for meiotic DSB resection, for antagonizing KU proteins, and for efficient recruitment of EXO-1 in early pachytene (see Fig. S6 in the supplemental material).

We found no evidence for a role for HIM-6 in resection, down-

stream of MRX/N, in *C. elegans* meiosis. This contrasts with the observation that human MRN enhances BLM-DNA2 resection activity *in vitro* (56). These findings may indicate a different role for HIM-6 in *C. elegans* meiosis (51) compared to that in other organisms, or it may be that HIM-6's action is masked by the redundant resection activity of EXO-1.

Overall, the *mre-11(iow1)* mutant provides unique insight into how defects in DSB resection affect events in meiosis and created an opportunity to disentangle various redundant pathways regulating the repair of meiotic DSB in *C. elegans*.

ACKNOWLEDGMENTS

Some strains and clones were kindly provided by the *Caenorhabditis* Genetics Center, which is funded by the NIH Office of Research Infrastructure Programs (P40 OD010440), and the *C. elegans* Reverse Genetics Core Facility at UBC, which is part of the International *C. elegans* Gene Knockout Consortium. We thank S. Boulton for the MRE-11 antibody, M. Hengartner for the RPA-1::YFP strain, and R. Chan for sharing protocols. We thank the Radiation and Free Radical Research Core Facility in the Carver College of Medicine for the irradiation service. We are grateful to R. E. Malone, J. A. Weiner, and members of the Smolnik lab for critical reading of the manuscript.

This work was supported by National Science Foundation grant MCB-1121150 (to S.S.) and UI startup funds (to S.S.).

REFERENCES

- Keeney S, Giroux CN, Kleckner N. 1997. Meiosis-specific DNA double-strand breaks are catalyzed by Spo11, a member of a widely conserved protein family. *Cell* 88:375–384.
- Neale MJ, Pan J, Keeney S. 2005. Endonucleolytic processing of covalent protein-linked DNA double-strand breaks. *Nature* 436:1053–1057.
- Mimitou EP, Symington LS. 2008. Sae2, Exo1 and Sgs1 collaborate in DNA double-strand break processing. *Nature* 455:770–774.
- Zhu Z, Chung WH, Shim EY, Lee SE, Ira G. 2008. Sgs1 helicase and two nucleases Dna2 and Exo1 resect DNA double-strand break ends. *Cell* 134:981–994.
- Gasior SL, Wong AK, Kora Y, Shinohara A, Bishop DK. 1998. Rad52 associates with RPA and functions with rad55 and rad57 to assemble meiotic recombination complexes. *Genes Dev.* 12:2208–2221.
- Shinohara A, Ogawa H, Ogawa T. 1992. Rad51 protein involved in repair and recombination in *S. cerevisiae* is a RecA-like protein. *Cell* 69:457–470.
- Sung P. 1994. Catalysis of ATP-dependent homologous DNA pairing and strand exchange by yeast RAD51 protein. *Science* 265:1241–1243.
- Schwacha A, Kleckner N. 1995. Identification of double Holliday junctions as intermediates in meiotic recombination. *Cell* 83:783–791.
- Johzuka K, Ogawa H. 1995. Interaction of Mre11 and Rad50: two proteins required for DNA repair and meiosis-specific double-strand break formation in *Saccharomyces cerevisiae*. *Genetics* 139:1521–1532.
- Tsubouchi H, Ogawa H. 1998. A novel *mre11* mutation impairs processing of double-strand breaks of DNA during both mitosis and meiosis. *Mol. Cell. Biol.* 18:260–268.
- Young JA, Hyppa RW, Smith GR. 2004. Conserved and nonconserved proteins for meiotic DNA breakage and repair in yeasts. *Genetics* 167:593–605.
- Hartsuiker E, Mizuno K, Molnar M, Kohli J, Ohta K, Carr AM. 2009. Ctp1CtIP and Rad32Mre11 nuclease activity are required for Rec12Spo11 removal, but Rec12Spo11 removal is dispensable for other MRN-dependent meiotic functions. *Mol. Cell. Biol.* 29:1671–1681.
- Puizina J, Siroky J, Mokros P, Schweizer D, Riha K. 2004. Mre11 deficiency in Arabidopsis is associated with chromosomal instability in somatic cells and Spo11-dependent genome fragmentation during meiosis. *Plant Cell* 16:1968–1978.
- Furuse M, Nagase Y, Tsubouchi H, Murakami-Murofushi K, Shibata T, Ohta K. 1998. Distinct roles of two separable *in vitro* activities of yeast Mre11 in mitotic and meiotic recombination. *EMBO J.* 17:6412–6425.
- Usui T, Ohta T, Oshiumi H, Tomizawa J, Ogawa H, Ogawa T. 1998.

- Complex formation and functional versatility of Mre11 of budding yeast in recombination. *Cell* 95:705–716.
16. Moreau S, Ferguson JR, Symington LS. 1999. The nuclease activity of Mre11 is required for meiosis but not for mating type switching, end joining, or telomere maintenance. *Mol. Cell. Biol.* 19:556–566.
 17. Rothenberg M, Kohli J, Ludin K. 2009. Ctp1 and the MRN-complex are required for endonucleolytic Rec12 removal with release of a single class of oligonucleotides in fission yeast. *PLoS Genet.* 5:e1000722. doi:10.1371/journal.pgen.1000722.
 18. Milman N, Higuchi E, Smith GR. 2009. Meiotic DNA double-strand break repair requires two nucleases, MRN and Ctp1, to produce a single size class of Rec12 (Spo11)-oligonucleotide complexes. *Mol. Cell. Biol.* 29:5998–6005.
 19. Garcia V, Phelps SE, Gray S, Neale MJ. 2011. Bidirectional resection of DNA double-strand breaks by Mre11 and Exo1. *Nature* 479:241–244.
 20. Luo G, Yao MS, Bender CF, Mills M, Bladl AR, Bradley A, Petrini JH. 1999. Disruption of mRad50 causes embryonic stem cell lethality, abnormal embryonic development, and sensitivity to ionizing radiation. *Proc. Natl. Acad. Sci. U. S. A.* 96:7376–7381.
 21. Zhu J, Petersen S, Tessarollo L, Nussenzweig A. 2001. Targeted disruption of the Nijmegen breakage syndrome gene NBS1 leads to early embryonic lethality in mice. *Curr. Biol.* 11:105–109.
 22. Ciapponi L, Cenci G, Ducau J, Flores C, Johnson-Schlitz D, Gorski MM, Engels WR, Gatti M. 2004. The Drosophila Mre11/Rad50 complex is required to prevent both telomeric fusion and chromosome breakage. *Curr. Biol.* 14:1360–1366.
 23. Gorski MM, Romeijn RJ, Eeken JC, de Jong AW, van Veen BL, Szuhai K, Mullenders LH, Ferro W, Pastink A. 2004. Disruption of Drosophila Rad50 causes pupal lethality, the accumulation of DNA double-strand breaks and the induction of apoptosis in third instar larvae. *DNA Repair* 3:603–615.
 24. Buis J, Wu Y, Deng Y, Leddon J, Westfield G, Eckersdorff M, Sekiguchi JM, Chang S, Ferguson DO. 2008. Mre11 nuclease activity has essential roles in DNA repair and genomic stability distinct from ATM activation. *Cell* 135:85–96.
 25. Lieber MR. 2010. The mechanism of double-strand DNA break repair by the nonhomologous DNA end-joining pathway. *Annu. Rev. Biochem.* 79:181–211.
 26. Heidenreich E, Novotny R, Kneidinger B, Holzmann V, Wintersberger U. 2003. Non-homologous end joining as an important mutagenic process in cell cycle-arrested cells. *EMBO J.* 22:2274–2283.
 27. Rothkamm K, Kuhne M, Jeggo PA, Lobrich M. 2001. Radiation-induced genomic rearrangements formed by nonhomologous end-joining of DNA double-strand breaks. *Cancer Res.* 61:3886–3893.
 28. Moore JK, Haber JE. 1996. Cell cycle and genetic requirements of two pathways of nonhomologous end-joining repair of double-strand breaks in *Saccharomyces cerevisiae*. *Mol. Cell. Biol.* 16:2164–2173.
 29. Symington LS, Gautier J. 2011. Double-strand break end resection and repair pathway choice. *Annu. Rev. Genet.* 45:247–271.
 30. Schiestl RH, Zhu J, Petes TD. 1994. Effect of mutations in genes affecting homologous recombination on restriction enzyme-mediated and illegitimate recombination in *Saccharomyces cerevisiae*. *Mol. Cell. Biol.* 14:4493–4500.
 31. Manolis KG, Nimmo ER, Hartsuiker E, Carr AM, Jeggo PA, Allshire RC. 2001. Novel functional requirements for non-homologous DNA end joining in *Schizosaccharomyces pombe*. *EMBO J.* 20:210–221.
 32. Di Virgilio M, Gautier J. 2005. Repair of double-strand breaks by non-homologous end joining in the absence of Mre11. *J. Cell Biol.* 171:765–771.
 33. Clejan I, Boerckel J, Ahmed S. 2006. Developmental modulation of nonhomologous end joining in *Caenorhabditis elegans*. *Genetics* 173:1301–1317.
 34. Martin JS, Winkelmann N, Petalcorin MI, McIlwraith MJ, Boulton SJ. 2005. RAD-51-dependent and -independent roles of a *Caenorhabditis elegans* BRCA2-related protein during DNA double-strand break repair. *Mol. Cell. Biol.* 25:3127–3139.
 35. Smollikov S, Eizinger A, Hurlburt A, Rogers E, Villeneuve AM, Colaiacovo MP. 2007. Synapsis-defective mutants reveal a correlation between chromosome conformation and the mode of double-strand break repair during *Caenorhabditis elegans* meiosis. *Genetics* 176:2027–2033.
 36. Chin GM, Villeneuve AM. 2001. *C. elegans* mre-11 is required for meiotic recombination and DNA repair but is dispensable for the meiotic G(2) DNA damage checkpoint. *Genes Dev.* 15:522–534.
 37. Hayashi M, Chin GM, Villeneuve AM. 2007. *C. elegans* germ cells switch between distinct modes of double-strand break repair during meiotic prophase progression. *PLoS Genet.* 3:e191. doi:10.1371/journal.pgen.0030191.
 38. Dernburg AF, McDonald K, Moulder G, Barstead R, Dresser M, Villeneuve AM. 1998. Meiotic recombination in *C. elegans* initiates by a conserved mechanism and is dispensable for homologous chromosome synapsis. *Cell* 94:387–398.
 39. Rinaldo C, Bazzicalupo P, Ederle S, Hilliard M, La Volpe A. 2002. Roles for *Caenorhabditis elegans* rad-51 in meiosis and in resistance to ionizing radiation during development. *Genetics* 160:471–479.
 40. Penkner A, Portik-Dobos Z, Tang L, Schnabel R, Novatchkova M, Jantsch V, Loidl J. 2007. A conserved function for a *Caenorhabditis elegans* Com1/Sae2/CtIP protein homolog in meiotic recombination. *EMBO J.* 26:5071–5082.
 41. Krogh BO, Llorente B, Lam A, Symington LS. 2005. Mutations in Mre11 phosphoesterase motif I that impair *Saccharomyces cerevisiae* Mre11-Rad50-Xrs2 complex stability in addition to nuclease activity. *Genetics* 171:1561–1570.
 42. Colaiacovo MP, MacQueen AJ, Martinez-Perez E, McDonald K, Adamo A, La Volpe A, Villeneuve AM. 2003. Synaptonemal complex assembly in *C. elegans* is dispensable for loading strand-exchange proteins but critical for proper completion of recombination. *Dev. Cell* 5:463–474.
 43. MacQueen AJ, Colaiacovo MP, McDonald K, Villeneuve AM. 2002. Synapsis-dependent and -independent mechanisms stabilize homolog pairing during meiotic prophase in *C. elegans*. *Genes Dev.* 16:2428–2442.
 44. Goodyer W, Kaitna S, Couteau F, Ward JD, Boulton SJ, Zetka M. 2008. HTP-3 links DSB formation with homolog pairing and crossing over during *C. elegans* meiosis. *Dev. Cell* 14:263–274.
 45. Hollingsworth NM, Ponte L, Halsey C. 1995. MSH5, a novel MutS homolog, facilitates meiotic reciprocal recombination between homologs in *Saccharomyces cerevisiae* but not mismatch repair. *Genes Dev.* 9:1728–1739.
 46. Kelly KO, Dernburg AF, Stanfield GM, Villeneuve AM. 2000. *Caenorhabditis elegans* msh-5 is required for both normal and radiation-induced meiotic crossing over but not for completion of meiosis. *Genetics* 156:617–630.
 47. Barnes TM, Kohara Y, Coulson A, Hekimi S. 1995. Meiotic recombination, noncoding DNA and genomic organization in *Caenorhabditis elegans*. *Genetics* 141:159–179.
 48. Tsai CJ, Mets DG, Albrecht MR, Nix P, Chan A, Meyer BJ. 2008. Meiotic crossover number and distribution are regulated by a dosage compensation protein that resembles a condensin subunit. *Genes Dev.* 22:194–211.
 49. Yokoo R, Zawadzki KA, Nabeshima K, Drake M, Arur S, Villeneuve AM. 2012. COSA-1 reveals robust homeostasis and separable licensing and reinforcement steps governing meiotic crossovers. *Cell* 149:75–87.
 50. Gartner A, Milstein S, Ahmed S, Hodgkin J, Hengartner MO. 2000. A conserved checkpoint pathway mediates DNA damage-induced apoptosis and cell cycle arrest in *C. elegans*. *Mol. Cell* 5:435–443.
 51. Wicky C, Alpi A, Passannante M, Rose A, Gartner A, Muller F. 2004. Multiple genetic pathways involving the *Caenorhabditis elegans* Bloom's syndrome genes him-6, rad-51, and top-3 are needed to maintain genome stability in the germ line. *Mol. Cell. Biol.* 24:5016–5027.
 52. Langerak P, Mejia-Ramirez E, Limbo O, Russell P. 2011. Release of Ku and MRN from DNA ends by Mre11 nuclease activity and Ctp1 is required for homologous recombination repair of double-strand breaks. *PLoS Genet.* 7:e1002271. doi:10.1371/journal.pgen.1002271.
 53. Mimitou EP, Symington LS. 2010. Ku prevents Exo1 and Sgs1-dependent resection of DNA ends in the absence of a functional MRX complex or Sae2. *EMBO J.* 29:3358–3369.
 54. Wu D, Topper LM, Wilson TE. 2008. Recruitment and dissociation of nonhomologous end joining proteins at a DNA double-strand break in *Saccharomyces cerevisiae*. *Genetics* 178:1237–1249.
 55. Lemmens BB, Johnson NM, Tijsterman M. 2013. COM-1 promotes homologous recombination during *Caenorhabditis elegans* meiosis by antagonizing Ku-mediated non-homologous end joining. *PLoS Genet.* 9:e1003276. doi:10.1371/journal.pgen.1003276.
 56. Nimonkar AV, Genschel J, Kinoshita E, Polaczek P, Campbell JL,

- Wyman C, Modrich P, Kowalczykowski SC. 2011. BLM-DNA2-RPA-MRN and EXO1-BLM-RPA-MRN constitute two DNA end resection machineries for human DNA break repair. *Genes Dev.* 25:350–362.
57. Prinz S, Amon A, Klein F. 1997. Isolation of COM1, a new gene required to complete meiotic double-strand break-induced recombination in *Saccharomyces cerevisiae*. *Genetics* 146:781–795.
58. Chiolo I, Carotenuto W, Maffioletti G, Petrini JH, Foiani M, Liberi G. 2005. Srs2 and Sgs1 DNA helicases associate with Mre11 in different sub-complexes following checkpoint activation and CDK1-mediated Srs2 phosphorylation. *Mol. Cell. Biol.* 25:5738–5751.
59. Niu H, Chung WH, Zhu Z, Kwon Y, Zhao W, Chi P, Prakash R, Seong C, Liu D, Lu L, Ira G, Sung P. 2010. Mechanism of the ATP-dependent DNA end-resection machinery from *Saccharomyces cerevisiae*. *Nature* 467:108–111.
60. Brenner S. 1974. The genetics of *Caenorhabditis elegans*. *Genetics* 77:71–94.
61. Stergiou L, Eberhard R, Doukometzidis K, Hengartner MO. 2011. NER and HR pathways act sequentially to promote UV-C-induced germ cell apoptosis in *Caenorhabditis elegans*. *Cell Death Differ.* 18:897–906.
62. Fernandez AG, Mis EK, Bargmann BO, Birnbaum KD, Piano F. 2010. Automated sorting of live *C. elegans* using laFACS. *Nat. Methods* 7:417–418.